Optica Applicata, Vol. XXXI, No. 1, 2001

Discontinuous metal films on dielectric substrates, their optical and electrical properties, structures and statistical descriptions

EWA DOBIERZEWSKA-MOZRZYMAS, PIOTR BIEGAŃSKI, EMILIA PIECIUL

Institute of Physics, Wrocław University of Technology, Wybrzeże Wyspiańskiego 27, 50–370 Wrocław, Poland.

A brief survey of some results concerning optical and electrical properties of discontinuous metal films on dielectric substrates and their statistical description is given. Optical properties (transmittance and imaginary part of dielectric permittivity spectra) of Al, Cu and Mn discontinuous films are presented and interpreted in terms of effective medium theories; modified Maxwell–Garnett and Bruggeman. The ranges of dielectric properties, the percolation threshold, and the range of metallic properties are determined for optical and electrical properties of the film examined. The considerations concerning electrical properties include such conduction mechanisms as metal conduction, substrate conduction, quantum tunneling, thermally activated tunneling and hopping. Real structures of the films are examined making use of electron microscope. Also the computer model for determining the contribution of the fundamental conduction mechanisms in discontinuous films is introduced. The inverse power law is used to describe the structure and the statistical distributions of inhomogeneous films of Au, Cu, and Mn on dielectric substrates. To this end, the rank of an island is connected with its area for the films with different coverage coefficients (metal content). The dependencies of the island areas on the rank orders in a double-logarithmic plot are straight lines according to the Mandelbrot law. The slope of the straight line characterises the ranges of the distributions of the islands: i) the log-normal or the Gaussian one (with two parameters of statistical distribution – the mean value and the variance), ii) the Poisson distribution (with one parameter – the mean value), iii) Lévy stable distribution (the parameters of distribution are infinite). The correlation between optical and electrical properties of discontinuous metal films and their structures and statistical description is found.

1. Introduction

The study of the physical properties, especially optical and electrical, and of the structures of discontinuous metal films on dielectric substrates is interesting from the viewpoint of both basic research and applications. Characterization of the structure of granular systems and their statistical description is one of the most important steps towards understanding their physical properties.

This paper describes some results concerning optical and electrical properties of discontinuous metal films on dielectric substrates. Optical properties of Al, Cu and Mn are presented and interpreted in terms of effective medium theories; Maxwell–Garnett, and Bruggeman (Sec. 2) The considerations concerning electrical properties include such conduction mechanisms as metal conduction, substrate conduction, quantum

tunneling, thermally activated tunneling and hopping (Sec. 3). The range of dielectric properties, the percolation threshold and the range of metallic properties are determined for optical and electrical properties (Sec. 2 and 3). The inverse power law is used to describe the structure and the statistical distributions of inhomogeneous films. Three kinds of statistical distributions are considered:

i) with two parameters of statistical distributions – the mean value and the variance,

ii) with one parameter – the mean value,

iii) without distribution parameters – mean value and variance are infinite (Sec. 4).

The correlation between optical and electrical properties of discontinuous metal films, their structure and statistical description is found.

2. Optical properties

2.1. Discrete island films

Experiments on the optical properties of cermets and discontinuous metal films prepared on dielectric substrates have been reported a number of times in recent years by Doremus, Jarrett and Ward, Truong and Scott, Bedeaux and Vlieger, Gadenne and Lafait, Yagil and Deutscher, Niklasson, Granqvist, Hunderi, Yamaguchi, Dobierzewska-Mozrzymas, Biegański *et al.* Optical properties of granular and discontinuous metal films differ from those of bulk media and of continuous films. The transmittance and reflectance spectra are generally characterized by the presence of absorption peaks, their position is dependent on on the quantity of the evaporated metal mass. Such absorption peaks are not observed for either a bulk metal or continuous films, they are not connected with the band structure of the metals.

Classical models are available to describe the optical properties of dispersion systems. In these models, metal islands deposited on dielectric substrates influenced by external electromagnetic field are assumed to form a system of dipoles. The theoretical approach of Maxwell–Garnett was the first to describe the problem. For spheroidal particles, when island diameter is much smaller than wavelength, effective permittivity ε' of discontinuous film may be determined by the expression [1]

$$\frac{\varepsilon'-\varepsilon_d}{\varepsilon'+2\varepsilon_d} = q\frac{(\varepsilon-\varepsilon_d)}{(\varepsilon+2\varepsilon_d)} \tag{1}$$

where: ε is the dielectric permittivity of the metal, ε_d is the dielectric permittivity of the medium surrounding the islands, which can be written as $\varepsilon_d = m\varepsilon_0+(1-m)\varepsilon_s$, $0 \leqslant m \leqslant 1$, where ε_0, ε_s is the air and the substrate permittivity, respectively, m denotes mixing parameter [2], q is a volume fraction defined as the ratio of the volume of islands to the total film volume. A convenient form for effective parmittivity is the formula

$$\varepsilon' = \varepsilon_d\frac{1+(2/3)q\alpha}{1-(1/3)q\alpha} \tag{2}$$

where α denotes the polarizability.

This theory has been modified several times, *e.g.*, by DAVID [3], YAMAGUCHI [4], DOREMUS [5], JARRETT and WARD [6], NORRMAN, ANDERSSON, GRANQVIST *et al.* [7].

In the general case for ellipsoidal grains the polarizability takes the form

$$\alpha = f \sum_i \frac{\varepsilon - \varepsilon_d}{\varepsilon_d + \mathscr{L}^i(\varepsilon - \varepsilon_d)} \tag{3}$$

where: $\mathscr{L}^i$ denotes the appropriate depolarization factor and f takes on different values depending on the orientation of the particles. The depolarization factors are given by LANDAU and LIFSHITZ [8].

For a sphere $\mathscr{L} = 1/3$, for the films with low volume fractions, the islands are regular in shape and their cross-sections are nearly circular ($a = b \neq c$, a and b are the semiaxes of ellipsoids in the plane parallel to the substrate and c is the semiaxis perpendicular to the substrate).

The depolarization factor for oblate ellipsoids ($a = b > c$) takes the form

$$\mathscr{L}_z = (\gamma^{-3} + \gamma^{-1})[\gamma - \arctan(\gamma)] \tag{4}$$

where: $\gamma = [(a/c)^2 - 1]^{1/2}$, $\mathscr{L}_x = \mathscr{L}_y = \frac{1}{2}(1 - \mathscr{L}_z)$.

For low volume fractions ($q \simeq 0.2$), the mean crystallite radius of metal grains approaches 10 nm. In this case, the size effects affect the dielectric permittivity of the metal ε because of the relaxation time of the conduction electrons which is involved in the Drude theory.

A crystallite size-dependent relaxation time τ_s is clasically introduced by adding a corrective term to the inverse of the relaxation time τ_0 in the bulk metal [9]

$$\frac{1}{\tau_s} = \frac{1}{\tau_0} + \frac{v_F}{r}. \tag{5}$$

The term accounts for the diffuse scattering at the surface of the particle of radius r of the electrons that travel with the Fermi velocity v_F.

It is known from the literature that after exposure to air, on oxide layer forms on the metal. The thickness of such a surface layer depends on the kind of the metal and on the physical conditions, its dielectric permittivity ($\varepsilon_C(\lambda) = \varepsilon_{1C} - i\varepsilon_{2C}$) may be determined making use of ellipsometric methods.

The optical properties of island films with non-homogeneous particles (metallic cores surrounded by a dielectric shell) were considered by NORRMAN *et al.* [7] and by GRANQVIST [9]. To determine the polarizabilities of the ellipsoids, the volume fraction q/Ω is adopted on the basis of structural examinations, with Ω being the ratio between the volume of the inner and outer ellipsoid

$$\Omega = \left(\frac{r}{r + d'}\right)^3 \tag{6}$$

where r is the mean radius of islands determined from the micrographs, and d' is the

thickness of the oxide surface layer. Thus, it is assumed that the surface layer thickness is homogeneous.

On the basis of large experimental data Jarrett and Ward defined the imaginary part of effective dielectric permittivity included in the Maxwell–Garnett model by the following expression [10]:

$$\varepsilon_2' = \frac{q\varepsilon_2\varepsilon_d}{[\varepsilon_d+(\varepsilon_1-\varepsilon_d)F]^2+\varepsilon_2^2F^2} \tag{7}$$

where ε_1, ε_2 denote the real and imaginary part of the metal dielectric permittivity, respectively. In this model, structural factor F depends on th shape of the grains and on the interaction among them

$$F = \mathscr{L} - AV\varepsilon_0 \tag{8}$$

where A is a coefficient of interaction between the islands, V is the island volume, ε_0 denotes dielectric permittivity of air. As the films satisfy the condition $d < \lambda$, the imaginary part of dielectric permittivity of the film may be obtained by Wolter's approximation [11]

$$\varepsilon_2' = \frac{\lambda}{2\pi d} n_d \frac{1-R-T}{T} \tag{9}$$

where: n_d is the refractive index of the substrate, d denotes the film thickness, R and T are reflectance and transmittance, respectively.

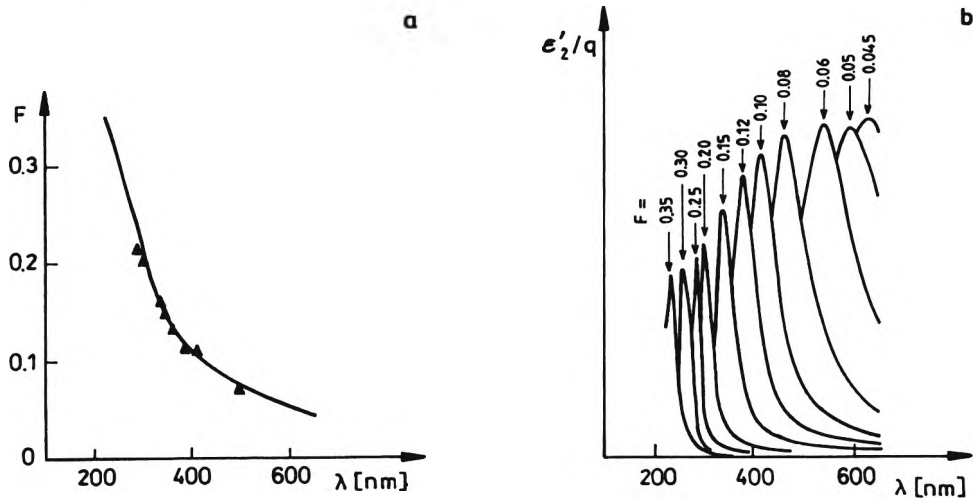

Fig. 1. Variation of factor F as a function of wavelength λ for Al films (Eqs. (7), (9)) — solid line, F vs. λ — triangles (a). Calculated value of ε_2'/q for Al films as a function of wavelength λ for selected values of factor F (b).

JARRETT and WARD [12] employed the following procedure to determine factor F. Considering the dependence of ε_2'/q vs. wavelength (Eq. (7), (9)), they found factor

F as a function of λ. This dependence is presented in Fig. 1**a** (solid line). To compare the values obtained by te above procedure with those obtained by our method, we calculated for Al films the ε_2'/q vs. λ (Eq. (7)) for selected values of F. The results are presented in Fig. 1**b**. For λ_{max} corresponding to the absorption peak, factor F was determined from F vs. λ_{max} (Fig. 1**a**, triangles). As shown by this curve, both methods give similar results for $0.30 \leqslant q \leqslant 0.40$ [13] Taking into account the approximate dependencies for ε_1 and ε_2 on wavelength on the basis of Drude theory, DOREMUS [14] showed that there are resonance effects of free electrons in individual grains that account for the absorption peak. The island films have a distinct absorption band, which shows a tendency to shift towards longer wavelength when the value of q increases.

For spherical grain particles Doremus proved that λ_{max} depends on volume fraction in the following way [14]:

$$\lambda_{max} = \lambda_c \left(\varepsilon_{st} + \frac{2+q}{1-q} n_s^2 \right)^{1/2} \tag{10}$$

where $\lambda_c^2 = (2\pi c)^2 m / 4\pi N_e e^2$.

In this expression, N_e, e, and m are the number, charge and mass of the free electrons, c is the velocity of light, ε_{st} is the frequency independent part of ε_1.

When the grains are assumed to be spheres or ellipsoids, the relationship between λ_{max} and F can be written as [13]

$$\lambda_{max} = \lambda_c \left[\varepsilon_{st} + n_s^2 \left(\frac{1}{F} - 1 \right) \right]^{1/2}. \tag{11}$$

Relations (10) and (11) make it possible to determine the position of the absorption peak when the structral parameters such as q or F are known from experimental measurements or fitted.

2.2. Aggregate films

Optical properties of discontinuous films with higher metal content (aggregate structure) may be interpreted in terms of the Bruggeman theory, renormalization approach proposed by Driss–Khodja and Berthier or scaling theory. According to the Bruggeman theory, the effective permittivity ε' of the film consisting of n components can be found from the equation [15]

$$\sum_{i=1}^{n} q_i \left(\frac{\varepsilon_i - \varepsilon'}{\varepsilon_i + 2\varepsilon'} \right) = 0 \tag{12}$$

where q_i is the volume fraction occupied by the i-th component and ε_i is its dielectric permittivity. Equation (12) describes optical properties of discontinuous films of the metals that partially oxidize during and after deposition.

To determine the optical properties (reflectance and transmittance spectra, real and imaginary part of the effective dielectric permittivity) of discontinuous films with higher volume fractions (near percolation threshold) Driss–Khodja and Berthier

proposed an effective medium theory based on the position space renormalization procedure [16]. This method applied to real digitized transmission electron micrographs or to randomly occupied square lattices generated by a computer.

The digitized transmission electron micrograph of a thin film is the initial square lattice of the process (size 512×512). Each pixel of the lattice has two possible states: a black one or a white one (metallic or dielectric, respectively). In the first step, the lattice is divided into blocks of four pixels (super pixels). The blocks and the method of determining the coverage coefficient p (ratio of metal covered surface to the total surface) are shown in paper [16]. Each block can be reduced to a unit cell with spherical or ellipsoidal inclusion (ε^i — dielectric permittivity) and to a matrix characterized by dielectric permittivity ε^{ma}. The inclusion shape is characterized by the depolarization factor $\mathscr{L}$. The dielectric permittivity of the super pixel is established in terms of the Maxwell–Garnett theory, which incorporates the size effect and island shape. After the first step the new super blocks are composed of four different constituents. The four components of any block in step n are reduced to two by an averaging process applied to the metallic-like components and to dielectric-like components, according to formula

$$\langle \varepsilon_n \rangle = \sum_j p_j \varepsilon_n^j \tag{13}$$

where j denotes the different components of metallic or dielectric class. For dielectric behaviour $\varepsilon_1 \approx \text{const} > 0$, ε_2 weak, for metallic behaviour $\varepsilon_1 < 0$, $\varepsilon_2 > 0$. Continuing with the renormalization process, the local effective dielectric function of the block is obtained in step n.

The computation is repeated for each super block of the lattice, and the whole process is repeated until the effective medium is obtained [16].

For higher volume fractions the metal islands produced by evaporation become irregular in shape, the structures of the films can be described by a fractal dimension at length scales less than a correlation length. Optical properties of such films can be interpreted in terms of the effective medium theory with structural parameter related to the fractal dimension. The formula obtained by Aspnes for effective dielectric permittivity of a two-phase material is the following [17]:

$$\varepsilon' = \frac{\varepsilon_A \varepsilon_B + 2\varepsilon_h (q_A \varepsilon_A + q_B \varepsilon_B)}{2\varepsilon_h + q_A \varepsilon_B + q_B \varepsilon_A} \tag{14}$$

where ε_A, ε_B and q_A, q_B denote the dielectric permittivities and volume fractions of materials A and B, respectively, ε_h is a dielectric permittivity of the surrounding in which the two materials are embedded. The following Bergman–Milton bounds are obtained [18], [19]:

$$\varepsilon_h = X\varepsilon_A + (1-X)\varepsilon_B, \tag{15}$$

$$\varepsilon_h^{-1} = X\varepsilon_A^{-1} + (1-X)\varepsilon_B^{-1}, \quad 0 \leqslant X \leqslant 1. \tag{16}$$

The structural parameter X is expressed by the pair correlation and three correlation function [20].

2.3. Aluminium, copper and manganese films

We undertook the examinations of the optical properties of aluminium, copper and manganese discontinuous films. Aluminium films were obtained by thermal evaporation with the pressure of 10^{-7} Pa. In each deposition process three Al films were evaporated, two films onto NaCl substrate for optical and structural studies, one on quartz substrate for thickness measurements. The thicknesses of the film, determined by multiple-beam interference method, were contained in the 11–42 nm range. On the basis of electron microscope examinations the volume fractions of the films were determined, they varied from 0.3 to 0.46. The transmittance T and the reflectance R spectra were measured in the 220–800 nm wavelength range. As the Al films under examination satisfied the condition $d < \lambda$, the imaginary part of dielectric permittivity ε_2 was obtained by Wolter's approximation (Eq. (9)). The results are presented in Fig. 2.

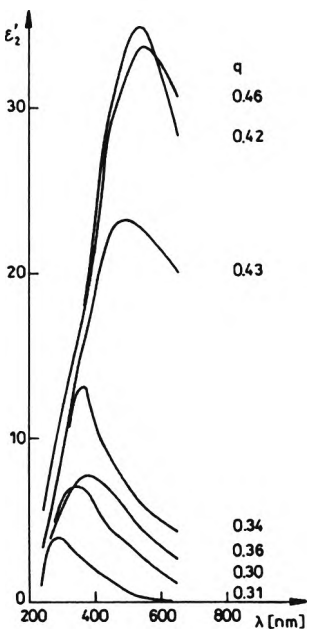

Fig. 2. Imaginary part od dielectric permittivity as a function of wavelength for Al films with different volume fractions.

It can be seen that the maximum of absorption has a tendency to shift towards longer wavelength. The increase of value q from 0.3 to 0.46 brought about a shift of the absorption peak from 290 to 550 nm. Using the method described above (Eq. (7), Fig. 1**a**, **b**, Eq. (11)) the dependence λ_{max} on structural factor F was determined, the result is presented in Fig. 3. It is shown that λ^2_{max} vs. $(1/F-1)$ is linear according to Eq. (11). It means that in the sense of modified Maxwell–Garnett theory, the value of λ_{max} depends both on the volume fraction q and the structural factor F which is a function of island shape and of interaction between them (Eq. (8)) [10].

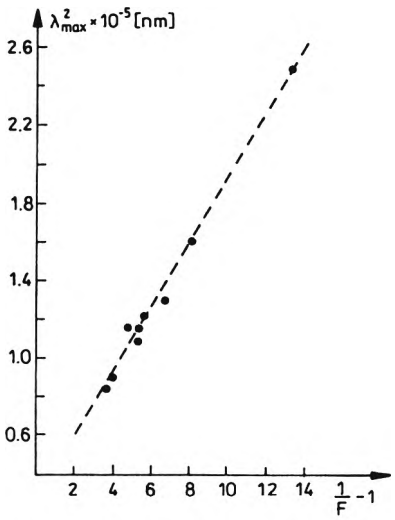

Fig. 3. The λ^2_{max} against $(1/F-1)$.

Copper films were thermally evaporated onto quartz substrates in vacuum (10^{-5} Pa) at an evaporation rate from 5 to 10 nm/s. Coverage coefficients p of the Cu films were determined on the basis of morphological examinations performed by electron microscope. Next, the volume fractions were calculated using the method described in paper [21]. The film thicknesses that were measured by the interference method were found to be from 10 to 30 nm.

The transmittance T for normal incidence was measured at wavelengths from 300 to 2500 nm by using a spectrophotometer. The transmittance spectra for films with different volume fractions are presented in Fig. 4. The plots show that the character

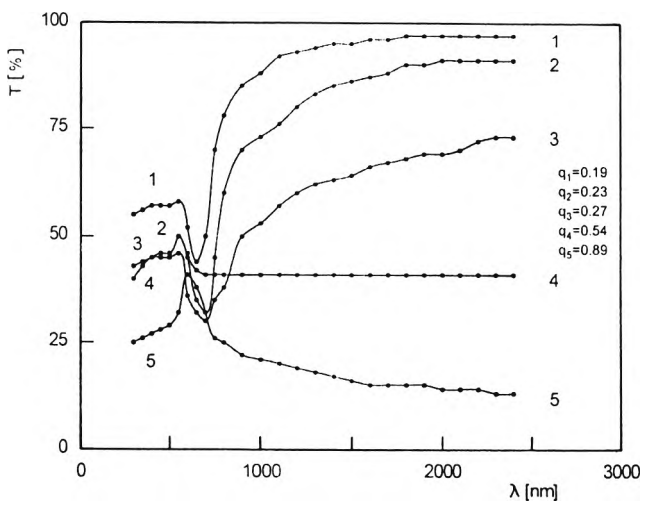

Fig. 4. Transmittance vs. wavelength in the visible range.

of the transmittance varies. Thus, for $q < q_c = q_4$, (q_c – critical volume fraction), the transmittance increase with wavelength. The plot is typical for a dielectric phase (q_1, q_2, q_3). In the visible range the curves reach the miniumum values T_{min}.

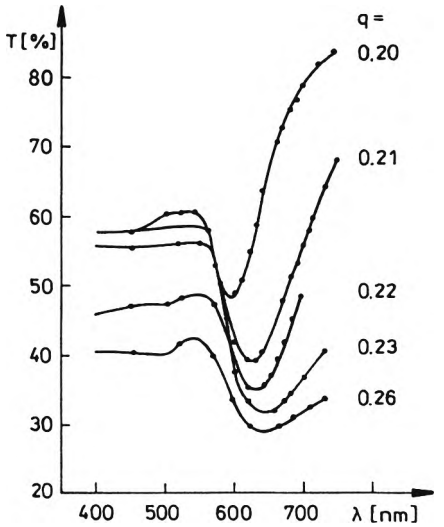

Fig. 5. Transmittance as a function of wavelength for Cu discontinuous films with different volume fractions.

In percolation threshold, for $q = q_c$, the transmittance in the IR range is independent of wavelength, the conduction path occurs in the film. When $q > q_c$, the plot is typical for a metallic phase q_5.

For the dielectric region, the minimum transmittance shifts towards longer wavelengths for the films of higher q values, as shown in Fig. 5. Similar behaviour has been reported for Au and Al discontinuous films [22]–[24]. By making use of Maxwell–Garnett theory, taking into consideration the grain shape (Eqs. (3), (4)), the size effect (Eq. (5)) and the surface oxide layer (Eq. (6)), the transmittances of the Cu films with low volume fractions were calculated. Examples of the results and measured data are plotted in Fig. 6**a**,**b**. The agreement between the theoretical and experimental results is good in the wavelength ranges that contain transmittance minima associated with the island structure of the films [21].

To interpret the optical properties (transmittance spectra) of Cu films with higher volume fractions, near and above percolation threshold, the renormalization approach was used. This method has been applied to digitized transmission electron micrographs for calculation of transmittance spectra.

The calculated results and measured data are plotted in Fig. 7**a**, **b**. In percolation ($q = 0.54$), the transmittance in the IR range is wavelength independent both in experimental and in the calculated curves (Fig. 7**a**). For volume fractions above the critical value, $q = 0.64$, we obtained very good agreement between theoretical and experimental results (Fig. 7**b**). The transmittance decreases at

longer wavelength; this plot is typical of the metallic phase. Using the renormalization method makes it possible to describe the transmittance spectra of discontinuous metal films with near percolation volume fractions [25].

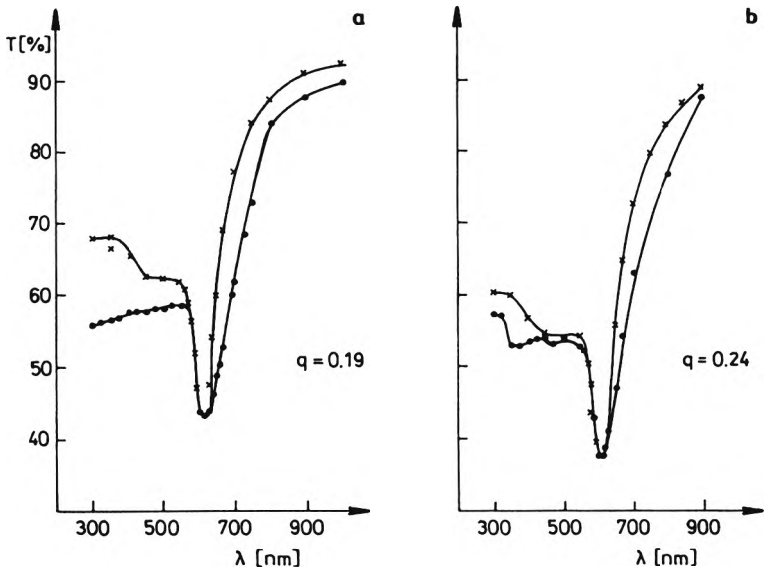

Fig. 6. Comparison of calculated (×) and measured (•) optical transmittance for island Cu films with different volume fractions: a — $q = 0.19$, b — $q = 0.24$.

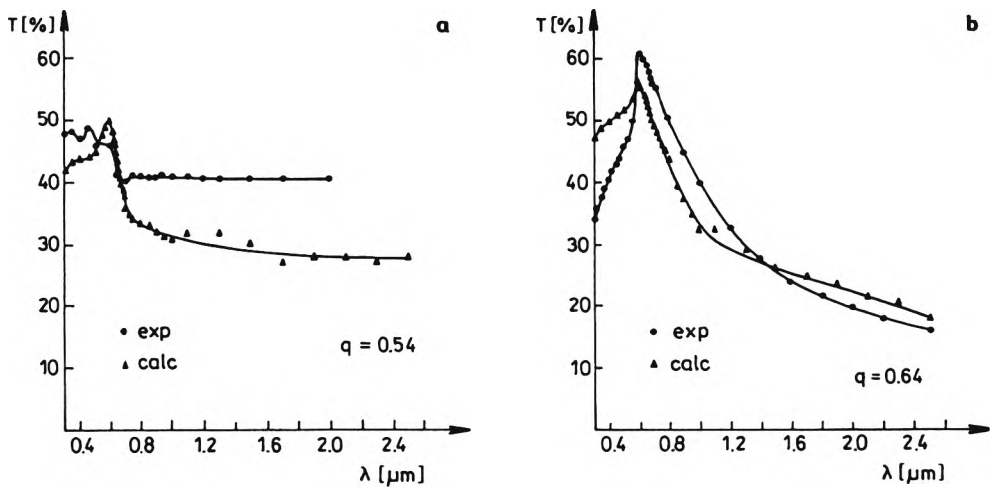

Fig. 7. Transmittance measured (•), (▲), and calculated by renormalization method (▲), (b) for Cu films with volume fractions near the percolation.

In the next stage, we investigated Mn discontinuous films; especially the influence of thermal annealing process on optical, electrical properties and on content and structure of the films. Two groups of Mn films with different mass thicknesses d_m

from 4 to 13 nm were evaporated onto quartz–glass substrates under vacuum conditions ($p = 10^{-5}$ Pa). The Mn films of the first group were thermally annealed at a temperature of approximately 690 K for half an hour. The films of the other group were obtained without thermal annealing. The microstructures and crystallographic orientations were examined by electron microscope. It has been found that the films of the first group consist of Mn small grains and MnO grains, the films of the second one exhibit aggregate structure. Transmittance spectra for both groups of Mn films with different thicknesses were measured in the wavelength range from 250 to 2500 nm. The results are preseneted in Fig. 8. The characters of the curves corresponding to the first and to the second group differ ones from anothers. In the annealed case, the transmittance distinctly decreases in the UV range; in the visible and IR it is approximately independent of wavelength. For unannealed films the transmittance

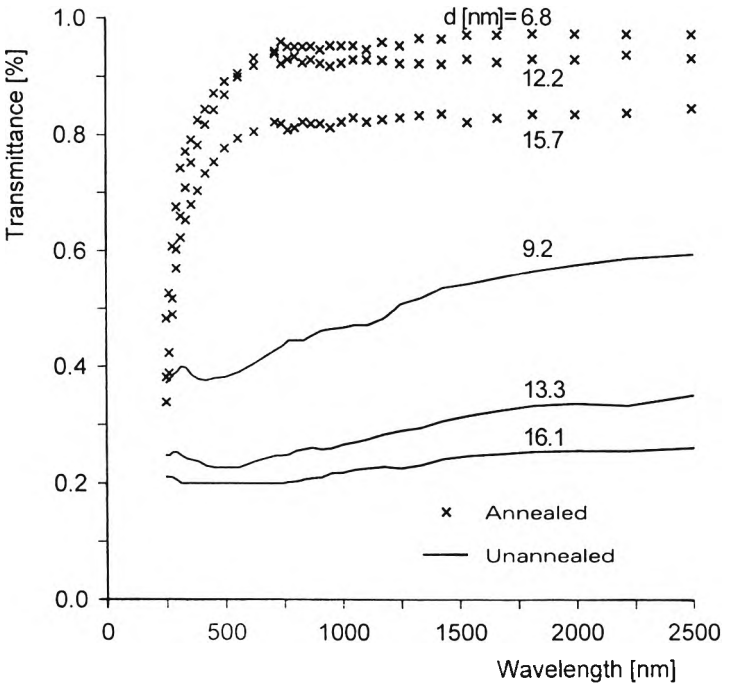

Fig. 8. Measured transmittance spectra for annealed and unannealed Mn films.

increases towards longer wavelength. To explain the optical properties of Mn films, the effective medium theories were applied; for annealed films the Maxwell–Garnett (Eq. (1)) and Bruggeman (Eq. (12)), for unannealed ones, with aggregated structure, the Bruggeman theory. A size effect was taken into consideration in the dielectric permittivity of the metal ε. Volume fractions q_{Mn} and q_{MnO} were determined from electron micrographs, ε_0 and m (mixing parameter) refer to the MnO content. The transmittance spectra were calculated, and the results are presented in Fig. 9**a**,**b**, together with experimental ones. A comparison between these curves shows for

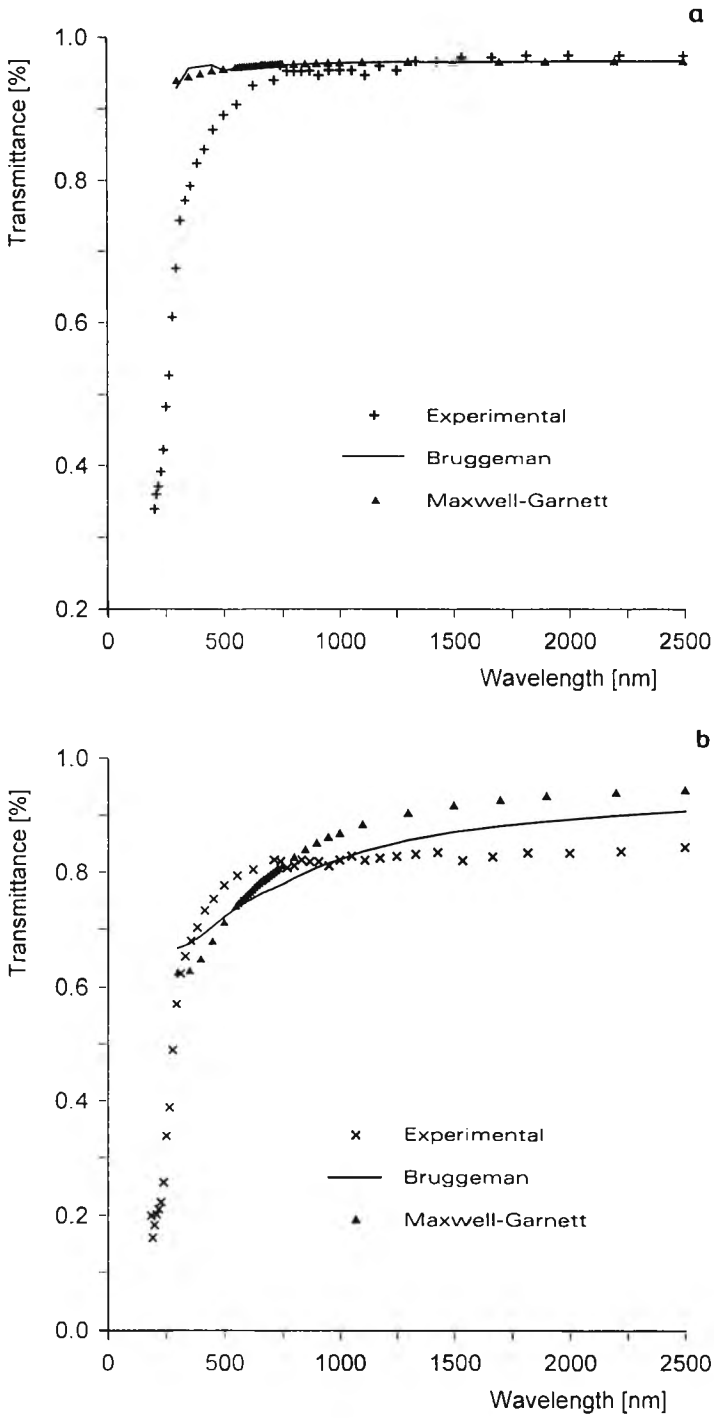

Fig. 9. Measured and calculated transmittance spectra for annealed Mn films: a – $d = 6.8$ nm, $q_{Mn} = 0.03$, $q_{MnO} = 0.186$, **b** – $d = 15.7$ nm, $q_{Mn} = 0.17$, $q_{MnO} = 0.64$.

annealed films a good agreement in the visible and IR range. In UV transmittance values decrease more rapidly than calculated ones. This discrepancy may be connected with light scattering. The Maxwell–Garnett as well as Bruggeman theory are suitable to explain the optical properties of annealed films which consist of Mn and MnO grains. The measured transmittance spectra and calculated ones in terms of Bruggeman theory for unannealed films are presented in Fig. 10. In the calculation the volume fractions of Mn were assumed as fitted parameters. Their values are

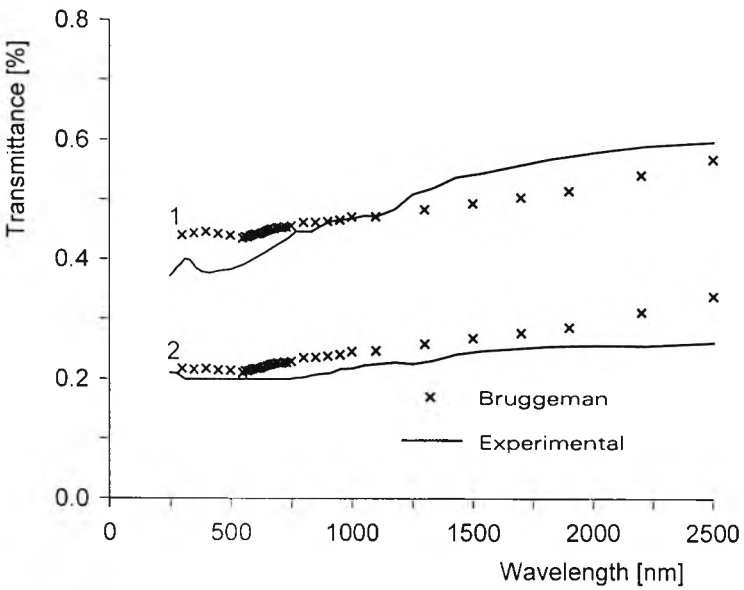

Fig. 10. Measured and calculated transmittance spectra for unannealed Mn films: 1 – $d = 9.2$ nm, $q_{\mathrm{Mn\ fit}} = 0.90$, $q_{\mathrm{Mn\,meas}} = 0.72$, $q_{\mathrm{MnO}} = 0.05$, $q_{\mathrm{air}} = 0.05$, 2 – $d = 16.1$ nm, $q_{\mathrm{Mn\ fit}} = 0.98$, $q_{\mathrm{Mn\ meas}} = 0.95$, $q_{\mathrm{MnO}} = 0.02$.

higher than those determined from the micrographs. It is probable that part of the metal is invisible on the micrographs. There is a good agreement between measured and calculated curves; Bruggeman theory explains optical properties of unannealed Mn films which exhibit aggregated structure. It has been found that the size effect is not essential for the first and second group of the films. Manganese is a transition metal, its relaxation time τ_0 is relatively short, and that is why the second term in relation (5) is small in comparison with the first one. In this case, the size effect do not affect the dielectric permittivity of the metal, differently as in the case of noble metals [26], [27].

3. Electrical properties

The electrical properties of metal discontinuous films on dielectric substrates are investigated using percolation models [28]–[30]. A metal island film deposited on

a dielectric substrate may be regarded as a system of randomly distributed metallic and dielectric regions.

The electric resistance of the film depends on the amount of deposited metal which is described by the coverage coefficient p (coverage coefficient is defined as the ratio of the metal surface to the total film surface). Making use of theoretical results and experimental data, it is possible to identify two distinct resistance regions. These are separated by the percolation threshold, which can be expressed in terms of the critical coverage coefficient p_c. The resistance of metal discontinuous films is a function of the coverage coefficient and may be expressed as [28], [29]

$$R(p) = R_D(p_c - p)^x, \quad \text{for } p < p_c, \tag{17}$$

or written as

$$R(p) = R_m(p - p_c)^{-t}, \quad \text{for } p > p_c \tag{18}$$

where R_D and R_m are the resistances of the system with all the bonds removed ($p = 0$) or with all the bonds present ($p = 1$), respectively, and x and t are the critical exponents. For the critical coverage coefficient p_c, the resistance of the discontinuous film may take the form

$$R(p_c) = R_m\left(\frac{R_D}{R_m}\right)^s \tag{19}$$

where s is the critical exponent given by

$$s = \frac{t}{x+t}. \tag{20}$$

The region described by Eq. (17) is characterizd by a high resistance, a negative temperature coefficient of resistance (TCR) and by thermally activated conduction (region 1). The region defined by Eq. (18) exhibits conduction which is typical for the metal (region 2). Thus, the value of TCR in the vicinity of the percolation threshold should approach zero. In the percolation threshold the electrical properties of a film undergo variations.

The conduction in island metal film (region 1) is a complicated process because of the various transport mechanisms such as substrate conduction, thermally activated tunneling, hopping, quantum tunneling and metal conduction may be involved.

Activation energy for thermally activated tunneling may be expressed as

$$\varepsilon_{ta} = \frac{e^2}{4\pi\varepsilon_0\varepsilon_r r} \tag{21}$$

where e denotes the electron charge, ε_r, r — relative dielectric permittivity of the surrounding medium and the island radius, respectively [31]. With island dimension increase the activation energy decreases. This character of activation energy changes is observed from experimental results for many discontinuous metal films [31], [32]. The experimental results for Al, Cu and Mn are presented in

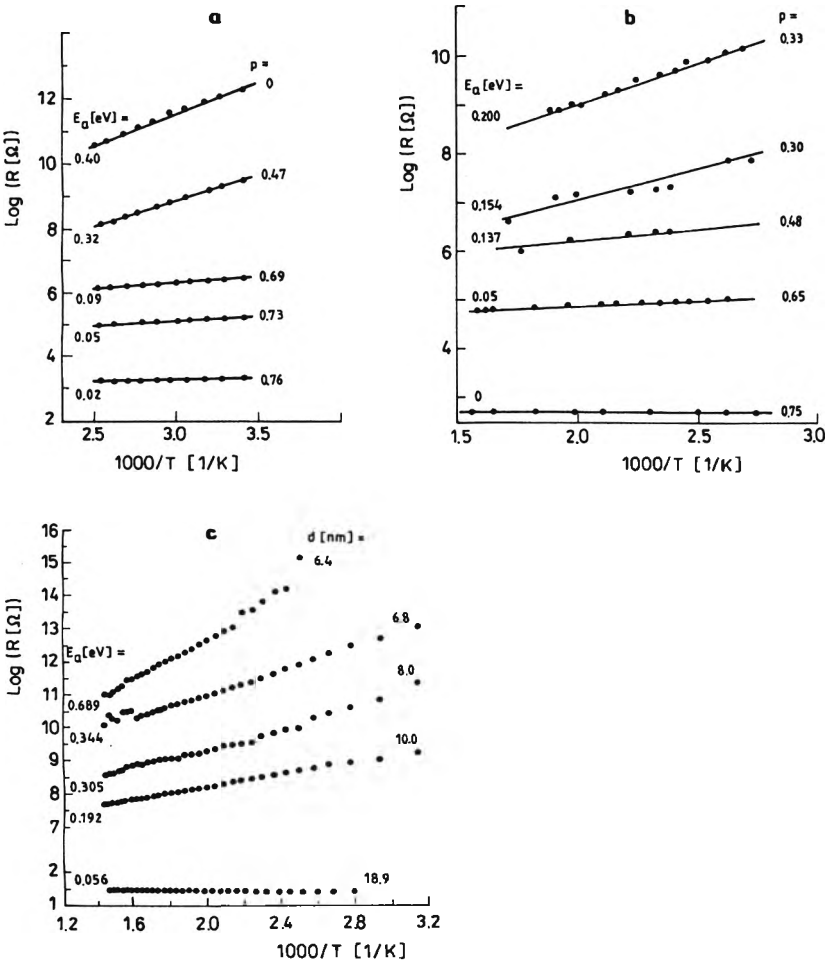

Fig. 11. Log(R) against 1000/T for the Al films with different coverage coefficients (**a**), for Cu films (**b**), for Mn films (**c**). (E_a denotes activation energy).

Fig. 11 **a**–**c**, respectively [33]–[35]. However, the activation energies determined on the basis of experimental data and relation (21) differ ones from others. This discrepancy may be connected with the appearance of another conduction mechanism, that is, hopping between microscopic localization centres. At low fields temperature dependencies of resistance take the form $\log(R) \sim T^{-\alpha}$, with constant α ranging from 1/4 to 1 depending on the temperature range and film structure. At a low temperature $\alpha = 1/4$, over a large range of higher temperatures $\alpha = 1/2$, and in a two dimensional medium $\alpha = 1/3$ [36].

To verify the occurrence of hopping conduction in discontinuous Mn films the plots of the log(R) vs. $T^{-1/2}$ were calculated for films with different thicknesses. The results are presented in Fig. 12, the dependencies are linear in the temperature range

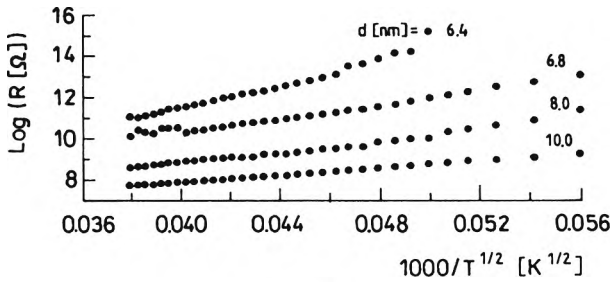

Fig. 12. Plot of $\log(R)$ vs. $T^{-1/2}$ for Mn films with different thicknesses.

under consideration. It is probable that the hopping conduction also occurs in Mn films examined [35].

For appropriate metal interisland spaces quantum tunneling conduction occurs, the tunneling resistance being defined by the following relation [37]:

$$R^t \sim \exp\left[\frac{4\pi L}{h}(2m\varphi)^{1/2}\right] \tag{22}$$

where L is the gap length, m is the electron mass, h is Planck's constant, φ denotes the potential barrier height for dielectric–metal system. The theories available which describe electrical properties of discontinuous films include only some of the conduction mechanisms, and the simplifications involved fail to provide sufficient agreement between calculated and measured data. For determining the contribution of the fundamental conduction mechanisms in discontinuous films a computer model was constructed. The model included metal conduction m, substrate conduction d, quantum tunneling t and thermally activated tunneling t_a. The computer modelled

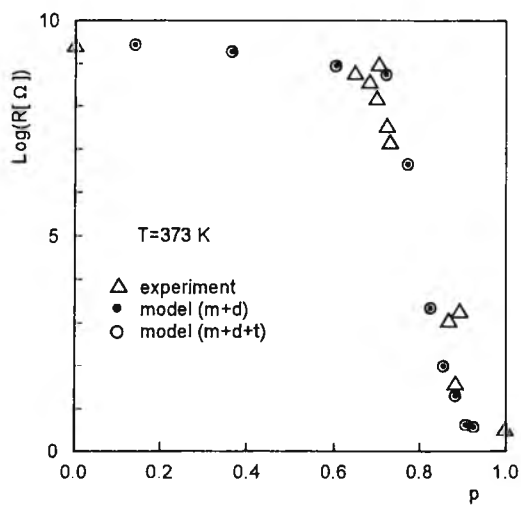

Fig. 13. Calculated and measured film resistance as a function of coverage coefficient for discontinuous Al films on NaCl substrates.

film structure is equivalent to real structure determined by microscopic examination. Making use of the computer method the dependencies of $\log(R)$ on coverage coefficient p for discontinuous Al films on NaCl were calculated at temperature $T = 373$ K. The measured and calculated results are presented in Fig. 13, the agreement is good as shown by the plots. There is no tunneling effect, the calculation results for model $m+d$ and $m+d+t$ are identical. The films for which the calculations have been performed displayed large islands and large gaps. Hence one can expect that the contribution of tunneling conduction will be small. This conduction mechanism gains importance for gap widths (barrier width) of a few angstroms. With all this in mind the dependence of $\log(R)$ on the p value for Al films displaying smaller islands and smaller gaps were calculated with and without tunneling. The mean sizes of the islands and the gaps have been assumed to be ten times smaller than those obtained from structural examinations. The results are plotted in Fig. 14. As shown by the calculated data, the contribution of this mechanism begins to increase in the case of fine-grain films with gap sizes amounting to a few angstroms [38]. Also, it is the tunneling conduction that makes the resistance in the percolation interval decrease less rapidly. This conduction may also apperar when small islands (invisible in the micrographs) are found in the gaps. The

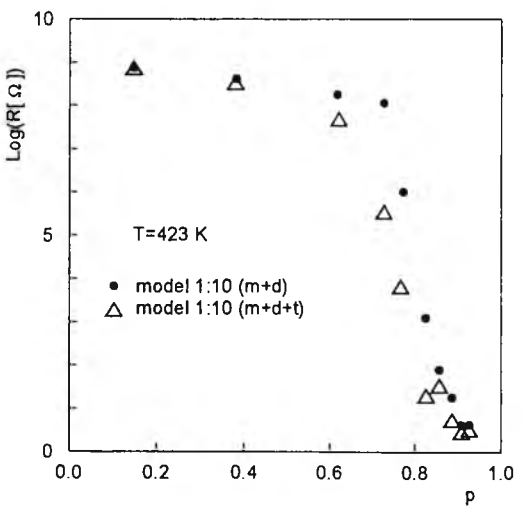

Fig. 14. Calculated film resistance as a function of coverage coefficient for different conduction mechanisms.

different changes of resistance in percolation threshold for Al and Cu films at temperature $T = 423$ K are presented in Fig. 15 **a,b**. The results for Al films were discussed in terms of the model of EFROS and SHKLOVSKI [28], whereas the critical index was determined by the method described by ABELES *et al.* [29]. Calculated resistance values on the coverage coefficient (solid line) are in good agreement with the experimental points (Fig. 15**a**). One can see that near the percolation threshold for Al films the resistance changes rapidly unlike in the case of Cu films

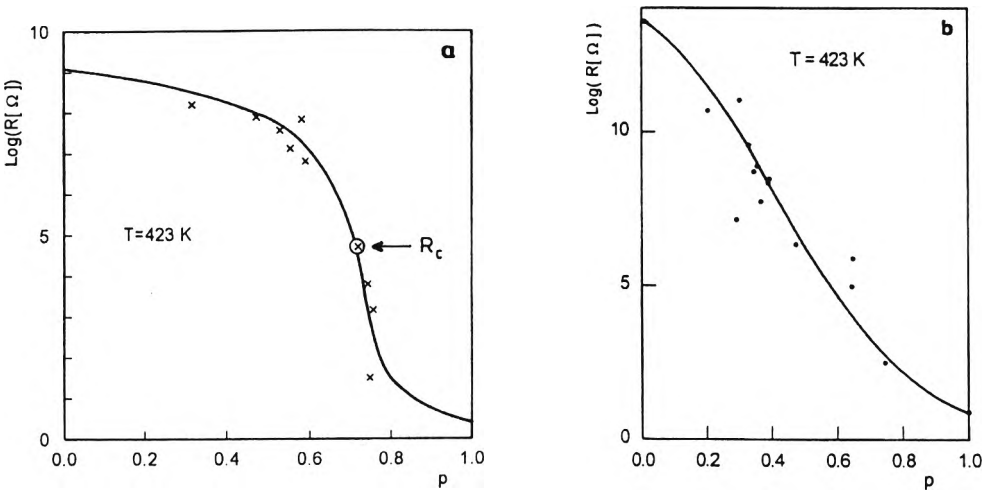

Fig. 15. Log(R) as a function of coverage coefficient: **a** — for Al films, **b** — for Cu films.

(Fig. 15**b**). This rapid variation is included in percolation model in which the discontinuous film is regarded as a mixture of dielectric and metallic phase. In the case of discontinuous Cu films the monotonic nature of the log(R) vs. p plot should be attributed to the occurrence of such conduction mechanisms as hopping and quantum tunneling. These conduction mechanisms are associated with the presence of small metal atom complexes or impurities in the gaps. Even through they are difficult to detect by structural studies, these factors have a noticeable effect on the electrical properties of the films. We used the resistance values measured under vacuum conditions to calculate the dependencies of the TCR on the coverage coefficient in the following regions: $p < p_c$, $q \approx q_c$ and $q > q_c$. The results for Al and Cu films are plotted in Fig. 16**a**,**b**, respectively. These curves behave differently depending on p value. Thus, when value p is smaller than q_c, the temperature dependence of the TCR becomes particularly distinct. The TCR takes negative values, which are to be atributed to the thermally activated mechanisms (thermally activated tunnelig, substrate conduction, hopping). When p approaches p_c, the TCR is slightly different from zero or equal to zero. For p greater than q_c, the TCR takes positive values and is temperature independent in the range examined. This emphasises the importance of metal conduction. From the plot of Fig. 16**a** it is possible to assess the interval of coverage coefficient Δq_c, in which the TCR approaches zero. This interval is approximately 0.70—0.73 [33]. The Cu film exhibits similar behaviour of the TCR. For lower p the TCR is negative, approaching zero in the range $0.60 \leqslant 0.75$. This range may be regarded as a percolation interval. For $q > 0.75$ the TCR is greater than zero and shows no temperature dependence.

We also examined the electrical properties of Mn discontinuous films. Two groups of the films with different mass thicknesses were evaporated onto quartz glass substrates under vacuum conditions ($p = 10^{-4}$ Pa). The Mn films of the first group were thermally anenaled at a temperature of approximately 674 K for half an hour.

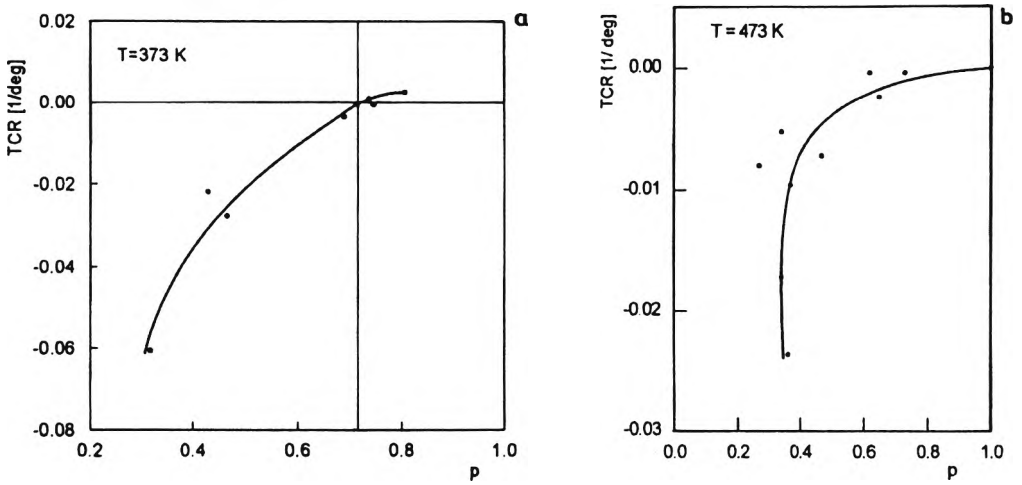

Fig. 16. The TCR as a function of coverage coefficient: **a** – for Al films, **b** – for Cu films.

The other group of films were obtained without thermal annealing. It has been found that electrical properties of the annealed Mn films differ from those of the films without annealing. The films of the first group reach higher resistance and higher activation energies of resistance values.

Figure 17**a**–**c** shows the relations between $\log(R)$ and $1000/T$ for annealed and unannealed films with mass thicknesses of approximately 5, 8 and 11 nm, respectively. The electrical properties of the thinnest films ($d \approx 5$ nm) of the first and second group are comparable. They exhibit high resistance over a considerable temperature range. The activation energies of resistance reach the value $E_a \approx$ 0.270 eV for both films (Fig. 17**a**).

In the case of films of middle thickness ($d \approx 8$ nm) the electrical properties of annealed films strongly differ from those of the film obtained without annealing.

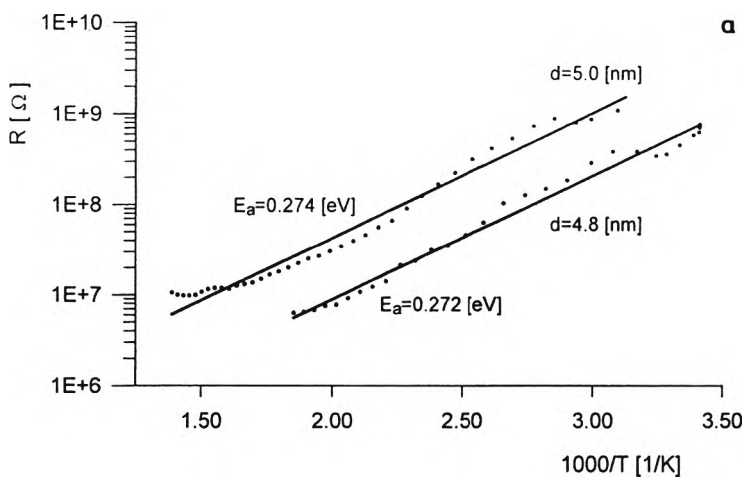

Fig. 17**a**

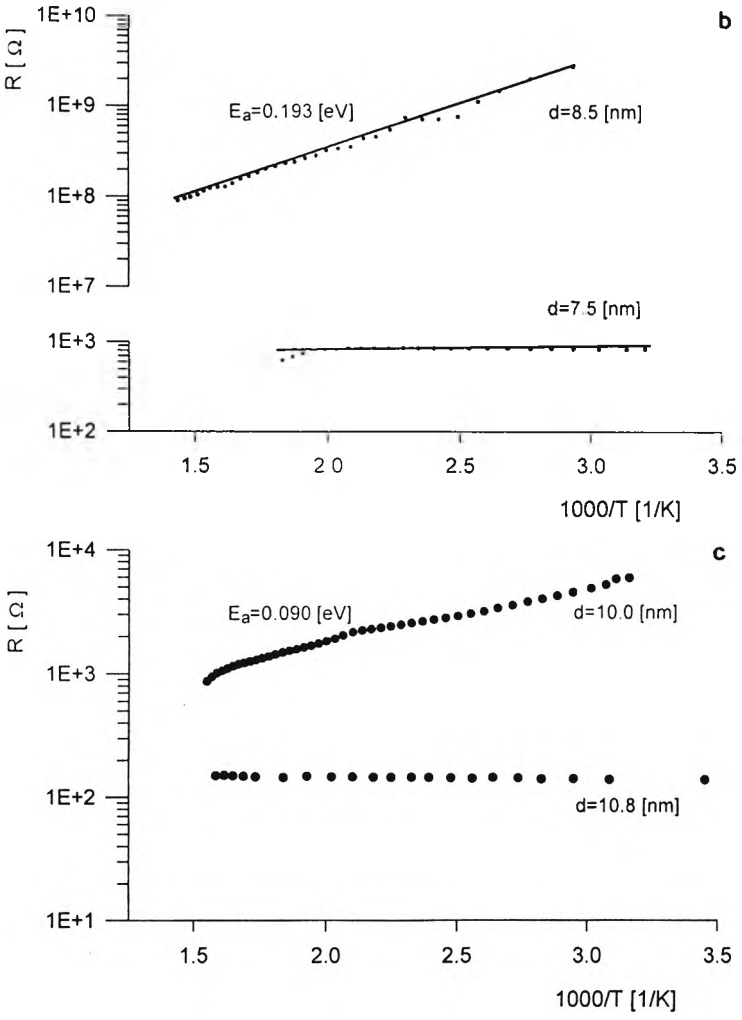

Fig. 17. Log(R) vs. 1000/T for Mn films with different thicknesses: **a** — $d \simeq 5$ nm, **b** — $d \simeq 8$ nm, **c** — $d \approx 11$ nm. Upper curves correspond to annealed films, bottom ones to unannealed films.

The film resistances of the former group are greater by several orders than those of the second group of approximately the same thicknesses. Also the activation energies differ, reaching the values 0.193 and 0 eV, respectively. The differences in electrical properties of thicker films of both groups are not so distinct as in the previous case. The activation energy of the annealed film $E_a = 0.09$ eV, and its resistance is more than one order higher than that of the unannealed one. The microstructure and crystallographic orientation were determined by means of electron microscope. The Mn films for structural examinations were obtained on copper grids (covered with formvar and amorphous carbon layer) under the same conditions as Mn films on quartz-glass substrates for electrical measurements. Structural examinations, especially indexed electron diffraction patterns show that

the films contain MnO [26]. One can suppose that oxidation processes occurring during and after evaporation of the films play a dominant role. The MnO domains cause high resistance of the thinnest films, resistivity of MnO $\rho \approx 10^{17} - 10^{19}$ Ωm (Fig. 17**a**). In the case of the middle thickness films, the oxidation processes during evaporation and annealing lead to the augmented MnO content in the film and cause the resistance and the activation energy increase (Fig. 17**b**). For thicker films oxidation during evaporation and particularly during annealing leads to increasing MnO content, but the conduction path of the metal exists in the thicker film, so its resistance is relatively small (Fig. 17**c**).

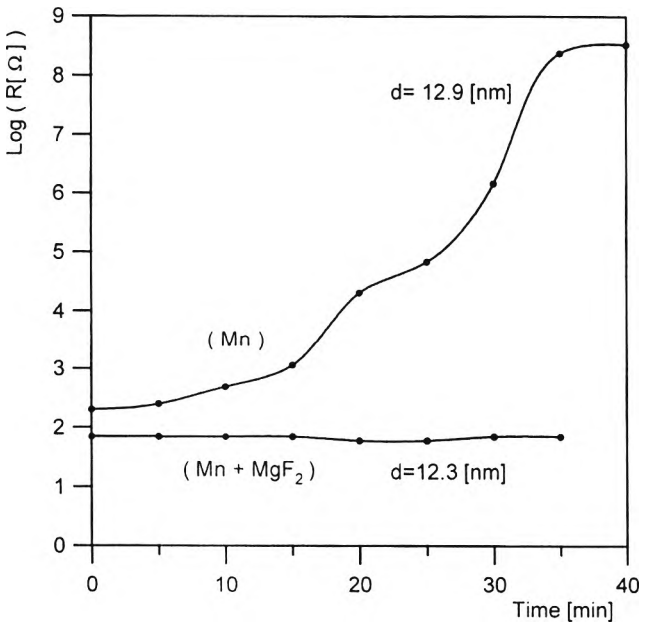

Fig. 18. Time dependencies of Mn film with thickness $d = 12.9$ nm and of double film ($d_{Mn} = 12.3$ nm, $d_{MnF_2} = 21$ nm).

To protect the Mn films against the oxidation process they were covered with dielectric layer (MgF_2) just after deposition, under vacuum conditions, their evaporation rate being about 0.1 – 0.5 nm/s, the thicknesses $d_d \approx 21$ nm. In order to examine the influence of MgF_2 layers on the electrical properties of Mn films, the time and temperature dependencies were measured under vacuum conditions. The results for Mn film and double film are shown in Fig. 18. The resistance of the double film is independent of time while for the Mn film it increases during annealing by several orders. Similarly, for the same thickness of the film the temperature dependencies of resistance of double and Mn films are different. For a given temperature, the resistance and activation energy of uncovered Mn film are higher than those of the film with dielectric layer, as shown in Fig. 19. The double films of thicknesses in the range 6 – 12 nm exhibit a percolative character, their resistances are independent of temperature [26].

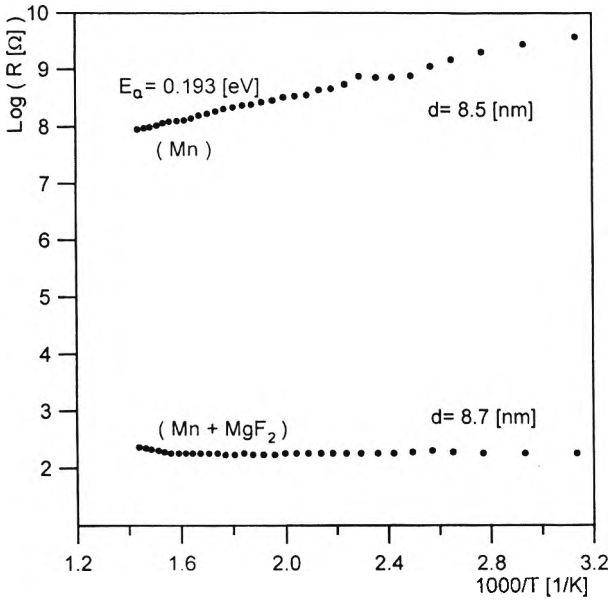

Fig. 19. Temperature dependencies of Mn film thickness $d = 8.5$ nm and of double film ($d_{Mn} = 8.7$ nm, $d_{MnF_2} = 21$ nm).

4. Structures and statistical description

Microscopic examinations performed by electron microscope reveal variations in film microstructure with increasing coverage coefficient. For low metal content the islands are regular in shape (spherical or ellipsoidal), when coverage coefficient increases they become more and more irregular and join together. In percolation a conduction path occurs in the film and its optical and electrical properties change.

Analyses of discontinuous film microstructures indicate that for higher coverage coefficients they exhibit fractal character, which is presented in the papers by FORREST and WITTEN [39], GADENNE *et al.* [40], NIKLASSON *et al.* [41], VOSS *et al.* [42], ORBACH [43], DOBIERZEWSKA-MOZRZYMAS *et al.* [44]. Examples of the structures corresponding to the films with different coverage coefficients are presented in Fig. 20**a**–**c**.

A statistical description of discontinuous film structure may be connected with Mandelbrot's law [45]. Let us consider a system consisting of the objects described by a random variable X; we can list the objects in the order of decreasing X value. The object with the largest variable value is ranked first, the next smaller value is ranked second, and so on. In this way we obtain the rank order k of the object.

Mandelbrot presented the general case of the power law in the form

$$X = \frac{1}{(k+\alpha)^{1+\beta}} \tag{23}$$

where α and β are constants.

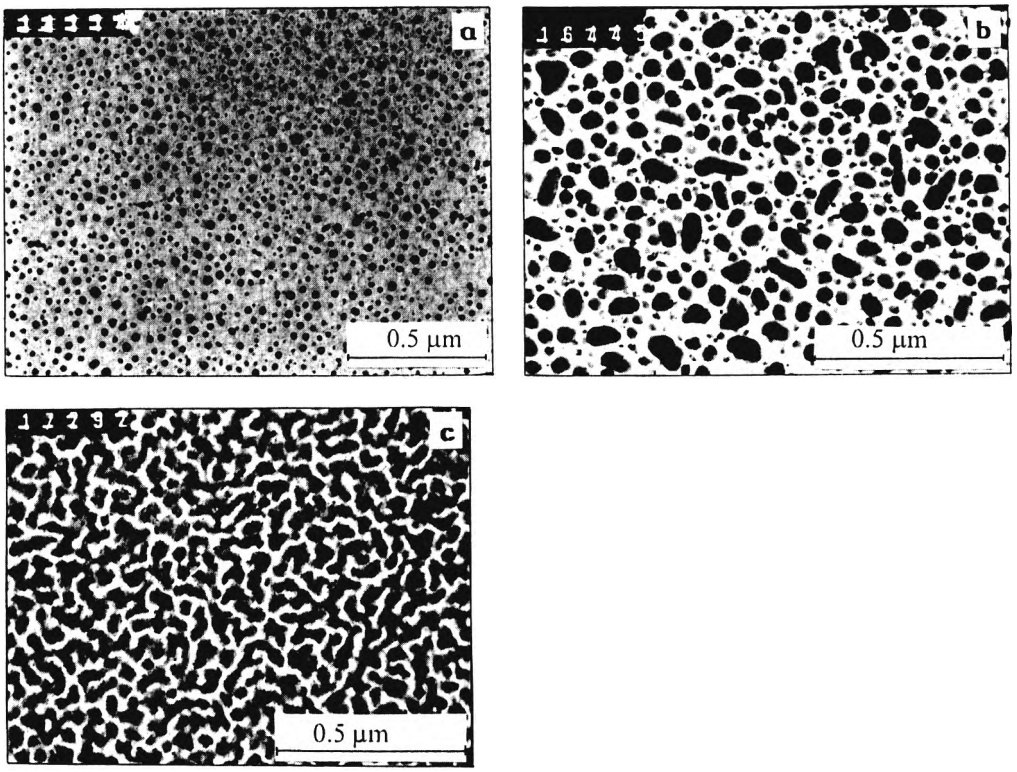

Fig. 20. Microstructures of discontinuous films: **a** — Cu film, $p = 30$, **b** — Cu film, $p = 0.39$, **c** — Mn film, $p = 0.62$.

When $\alpha = \beta = 0$, we obtain the Zipf's law

$$X = \frac{1}{k}, \tag{24}$$

which is satisfied, for example, in the case of the city populations and frequencies of occurrence of words in a piece of text [46].

BOUCHAUD [47] pointed out that there is a distinct correlation between the slope of the straight line representing the power law of Mandelbrot and the inhomogeneity of the system. The slope of straight line determined as $-1/\mu$ (μ denotes the critical exponent), characterizes the distribution of the elements in the structure.

The main property of the variable is that all its moments of q order are finite for $q \leqslant \mu$. Consequently, one can distinguish the following ranges of the critical exponent μ:

i) $\mu > 2$, the moment of the first order m_1 and the moment of the second order m_2 are finite. The ordinary moment m_1 equals the mean value, it is defined as

$$\bar{X} = \frac{1}{N} \sum_{i=1}^{N} X_i. \tag{25}$$

The central moment m_2 is a variance

$$\sigma^2 = \frac{1}{N}\sum_{i=1}^{N}(X_i - \bar{X})^2. \tag{26}$$

For this range of μ, the two parameters of the statistical distribution ($\bar{X}$ and σ^2) are finite, for large N the usual central-limit theorem applies; therefore the statistical distribution of the system tends towards a Gaussian or log-normal one.

ii) For $1 < \mu < 2$, inhomogeneity of the structure appears, and the moment of the first order is finite. For description of such system, a statistical distribution with one parameter (the mean value) may be used, for example, Poisson distribution.

iii) For $\mu < 1$, the "hierarchisation" of the structure is more pronounced, and the moments of the first and second order are infinite. For large N the objects are distributed according to the Lévy stable distribution. The system may also be described by making use of Pareto's statistical distribution; the structures become fractal.

For an appropriate greater slope of straight line a phase transition may occur. The increase of the angle between the straight line representing the inverse power law

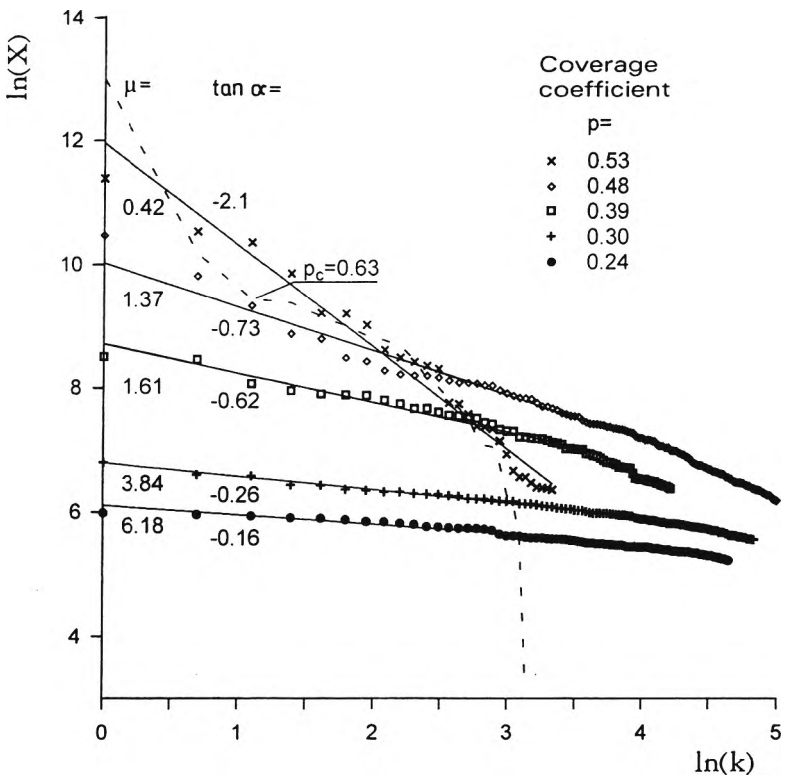

Fig. 21. Island area X vs. order rank k for films with different coverage coefficients in a double-logarithmic plot; the straight lines were fitted using the least-squares regression method.

and the rank axis (in logarithmic plot) determines the increase of the inhomogeneity of the system, and determines also the direction of evolution of the structure toward a phase transition.

The inverse power law may be used to described the structures and the statistical distributions of discontinuous metal films on dielectric substrates. To this end, the rank of an island k was connected with its area X for the films with different metal content (coverage coefficient). The ranges of the exponent μ determined correspond to different statistical descriptions of islands in discontinuous metal films. Using a special computer program the islands on the micrograph were ranged in order of decreasing island area. The results for the metal films with different coverage coefficients are presented in Fig. 21. The dependencies of the island area X on its rank order k in double-logarithmic plot, representing the power law of Mandelbrot (23), are straight lines. The slopes depend on the inhomogeneity of the structure, which is connected with the metal content. For coverage coefficients $p \leqslant 0.3$ the islands are regular in shape, their areas differ insignificantly. The slopes of these straight lines correspond to values $\mu > 2$ (case i). The parameters of the distribution such as the mean value and the variance are finite. These structures may be described by a statistical distribution using two parameters, for example, a Gaussian or log-normal distribution. Figure 22 shows an experimental and a calculated log-normal distribution. On the basis of structural examinations, the parameters of distribution, such as the mean value $\bar{X}$ and the variance σ^2 were determined.

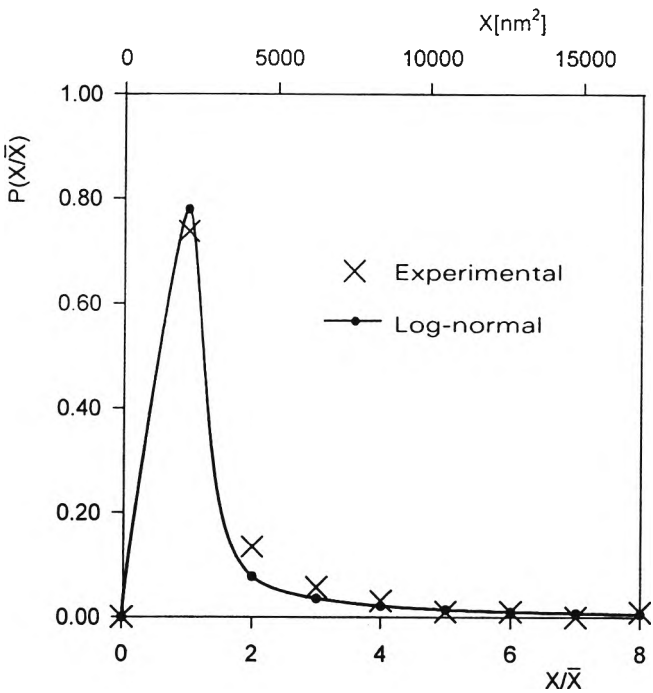

Fig. 22. Log-normal distribution of island areas for Cu film with coverage coefficient $p = 0.30$, a log-normal distribution with standard deviation $\sigma = 1.8$.

For these parameters the log-normal distribution was calculated. The experimental distribution obtained from the histograms of island areas is also presented. The agreement between the theoretical and experimental description is good. The statistics with two parameters may describe such structures.

With increasing metal content the islands become more irregular; they change shape from spherical to ellipsoidal and then to long paths along the film, as is seen in Fig. 20**a**–**c**. Also, the areas of the island are different. The experimental histograms presented in Figs. 23 and 24 show that, in addition to the islands with small areas, there are also the islands with very large areas. When $1 < \mu < 2$, the Poisson distribution describes the metal film structure. Experimental and theoretical results are compared in Fig. 23. The probability of the appearance of large islands is small,

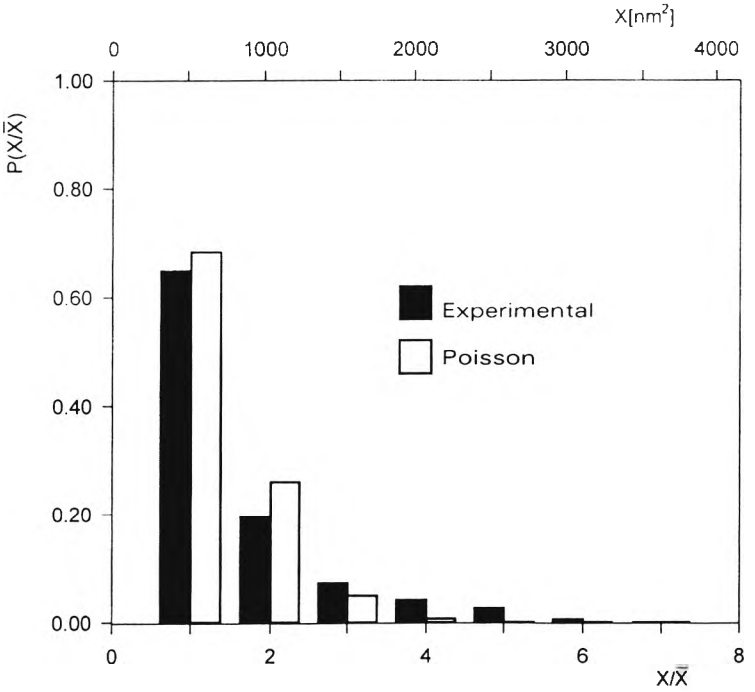

Fig. 23. Poisson distribution of island areas for Cu film with coverage coefficient $p = 0.39$.

but they do occur in the discontinuous films. In this case, the angle between the straight line representing the Mandelbrot law and the rank axis (in the logarithmic plot) increases, and the critical index is in the range $1 < \mu < 2$ or $\mu < 1$ (cases ii) and iii)). It is interesting that for $\mu \approx 1$ the entire sum is, in a first approximation, given by its largest term

$$\frac{X_1}{\sum_{i=2}^{N}} \approx 1. \tag{27}$$

In such a case the mean value $\bar{X}$ in fact loses its meaning. This is a key feature of the Lévy distribution. These structures exhibit self-similar properties; they become fractal. An experimental histogram of such structure is presented in Fig. 24. The islands with large areas occur in the discontinuous Mn film with the coverage coefficient $p = 0.62$. To describe this structure, Pareto's distribution was used. Comparison of the experimental results with calculated ones allows us to confirm that there is satisfactory agreement.

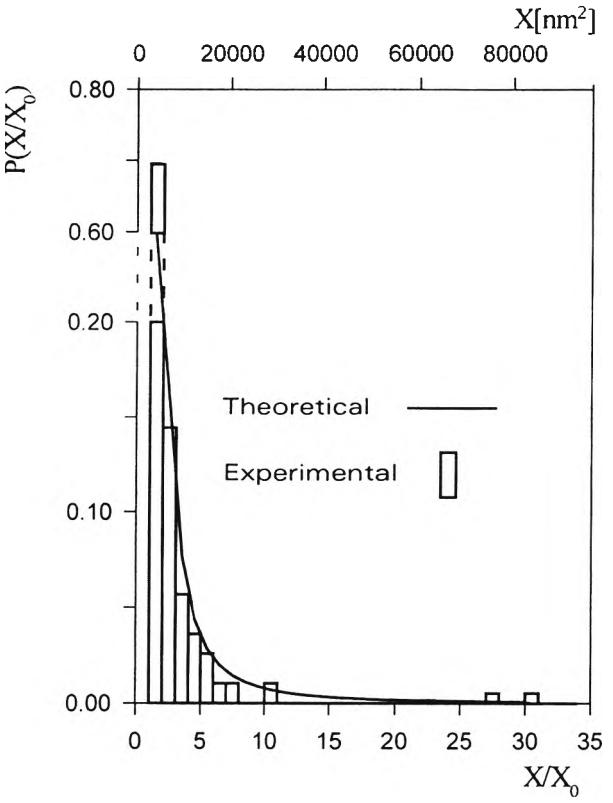

Fig. 24. Experimental distribution of island areas and Pareto's distribution of island areas for Mn film. Pareto's distribution is defined as follows: $\rho(X) = (\mu/X_0)(X_0/X)^{\mu+1}$ for $X > X_0$, where X_0 denotes a typical scale, and the smallest variable is of order X_0 [47].

In phase transition (at the percolation threshold), the infinite cluster appears, and the inverse law loses its validity. For the discontinuous Cu film, $p_c = 0.63$ (Fig. 21): for this value, the optical and electrical properties of Cu films change from dielectric to metallic ones [48].

5. Summary

As presented above, structures of discontinuous metal films correspond to their optical and electrical properties. The character of transmittance depends on volume

fraction of the films. For $q < q_c$ the transmittance increases with wavelength. In the visible range the curves reach the minima values typical for island films, for dielectric region (Figs. 4 and 5, for Cu films, curves q_1, q_2, q_2). For this region the maxima of imaginary part of dielectric permittivity are also typical, what is presented for Al films in Fig. 2. The transmittance minima show a tendency to shift towards longer wavelength when the q value increases.

The position of the absorption peak may be determined by structural parameter F which depends on the shape of the islands and on the interaction between them (Eq. (8), Fig. 3). When $q = q_c$, the optical anomalies (peaks) disappear and the transmittance in the IR is independent of wavelength (Fig. 4, curve $q_c = q_4$). This character of transmittance is connected with a phase transition from dielectric to metallic properties. For $q > q_c$ the plot is typical for metallic phase, the transmittance decreases with wavelength (Fig. 4, curve 5).

Similarly, one can distinguish three ranges of the electrical properties of discontinuous films. The dependence of $\log(R)$ on coverage coefficients makes it possible to determine dielectric range $(0-p_c)$, percolation threshold (p_c) and metallic region $(p > p_c)$. For coverage coefficient $p < p_c$ the films exhibit high resistance, thermally activated conduction mechanisms, the TCR of these films being negative. These properties are distinctly seen for Al films (Figs. 11**a**, 15**a**, and 16**a**). At threshold $p = p_c$, the electrical properties undergo significant variations; the resistance rapidly decreases, TCR ≈ 0 (Figs. 11**a**, 15, 16**a**). This behaviour is to be attributed to the change in the type of conduction, with the appearance of the conduction path in the film. For $p > p_c$ electrical properties are typical as for metallic phase; low resistance, the TCR is greater than zero.

In dielectric range the inverse power law connecting the island rank with its area is satisfied (Fig. 21). In terms of Mandelbrot's law one can distinguish the range of structures corresponding to different statistical descriptions. In transition from dielectric to metallic range the infinite cluster is formed, and the inverse power law is no longer valid (Fig. 21, $p = 0.63$).

Acknowledgments — This work was done for the Wrocław University of Technology under Contract No. 34237-7.

References

[1] MAXWELL-GARNETT J.C., Philos. Trans. R. Soc. **203** (1904), 385. *Ibidem*, **205** (1906), 237.
[2] DOBIERZEWSKA-MOZRZYMAS E., PEISERT J., BIEGAŃSKI P., Appl. Opt. **27** (1988), 181.
[3] DAVID E., Z. Phys. **144** (1939), 389.
[4] YAMAGUCHI S., J. Phys. Soc. Jpn. **17** (1962), 1172.
[5] DOREMUS R.H., J. Chem Phys. **40** (1964), 2389, **42** (1965), 414. DOREMUS R.H., Thin Solid Films **326** (1998), 205.
[6] JARRETT D.N., WARD L., J. Phys. D **9** (1976), 1515.
[7] NORRMAN S., ANDERSSON T., GRANQVIST C.G., HUNDERI O. Phys. Rev. B **18** (1978), 674.
[8] LANDAU L.D., LIFSHITZ E.M., *Electrodynamics of Continuous Media*, Pergamon, New York 1960, p. 27.
[9] GRANQVIST C.G., J. Phys. (Paris), Suppl. **42** C1 (1981), 247.
[10] JARRETT D.N., WARD L., J. Phys. D **9** (1976), 237.

[11] WOLTER H., Z. Phys. **105** (1937), 269. *Ibidem* **113** (1939), 547.
[12] WARD L., *The Optical Constants of Bulk Materials and Films*, [Ed.] A. Hilgier, Bristol, Philadelphia 1988.
[13] DOBIERZEWSKA-MOZRZYMAS E., RADOSZ A., BIEGAŃSKI P., Appl. Opt. **24** (1985), 727.
[14] DOREMUS R.H., J. Appl. Phys. **37** (1966), 2775.
[15] BRUGGEMAN D.A.G., Ann. Phys. (Leipzig) **24** (1935), 636.
[16] DRISS-KHODJA K., BERTHIER S., J. Phys. Condens. Matter **2** (1990), 8651.
[17] ASPNES D.E., Thin Solid Films **89** (1982), 249.
[18] BERGMAN D.J., Phys. Rev. Lett. **44** (1980), 1285.
[19] MILTON G.W., Appl. Phys. Lett. **37** (1980), 300.
[20] NIKLASSON G.A., J. Appl. Phys. **61** (1987), 258.
[21] DOBIERZEWSKA-MOZRZYMAS E., BIEGAŃSKI P., Appl. Opt. **32** (1993), 2345.
[22] GADENNE P., BEGHDADI A., LAFAIT J., Opt. Commun. **65** (1988), 17.
[23] YAGIL Y., DEUTSCHER G., Thin Solid Films **152** (1987), 465.
[24] KUNZ M., NIKLASSON G.A., GRANQVIST C.G., J. Appl. Phys. **64** (1988), 3740.
[25] DOBIERZEWSKA-MOZRZYMAS E., BIEGAŃSKI P., PIECIUL E., Vacuum **45** (1994), 279.
[26] *Ibidem*, **50** (1998), 35.
[27] DOBIERZEWSKA-MOZRZYMAS, WÓJCIK J., BIEGAŃSKI P., PIECIUL E., Vacuum **54** (1999), 299.
[28] EFROS A.L., SHKLOVSKII B.J., Phys. Status Solidi B **76** (1976), 475.
[29] ABELES B., PINCH H.L., GITTLEMAN J.I., Phys. Rev. Lett. **35** (1975), 247.
[30] STRALEY J.P., Phys. Rev. B **15** (1977), 5733.
[31] NEUGEBAUER C.A., WEBB M.B., J. Appl. Phys. **33** (1962), 74.
[32] CHOPRA L.L., *Elektricheskie yavleniya v tonkich plonkakh* (in Russian), Mir, Moscow 1972.
[33] DOBIERZEWSKA-MOZRZYMAS E., BIEGAŃSKI P., J. Phys. F, Met. Phys. **18** (1988), 2061.
[34] BIEGAŃSKI P., DOBIERZEWSKA-MOZRZYMAS E., Int. J. Electron. **70** (1991), 499.
[35] BIEGAŃSKI. P., DOBIERZEWSKA-MOZRZYMAS E., PIECIUL E., WÓJCIK J., Proc. SPIE **2780** (1996), 15.
[36] PING SHEN, KLAFTER J., Phys. Rev. B **27** (1983), 2583.
[37] HOLM R., J. Appl. Phys. **22** (1951), 569.
[38] BŁAŻEJ M., DOBIERZEWSKA-MOZRZYMAS E., Thin Solid Films **192** (1990), 219.
[39] FORREST S.R., WITTEN T.A., J. Phys. A **12** (1979), L109.
[40] GADENNE M., LAFAIT J., GADENNE P., Opt. Commun. **71** (1989), 273.
[41] NIKLASSON G.A., TOREBRING A., LARSSON C., GRANQVIST C.G., Phys. Rev. Lett. **60** (1988), 1735.
[42] VOSS R.F., LAIBOWITZ R.B., ALLESSANDRINI E.I., Phys. Rev. Lett. **39** (1982), 1441.
[43] ORBACH R., Science **231** (1986), 814.
[44] DOBIERZEWSKA-MOZRZYMAS R., BIEGAŃSKI P., WÓJCIK J., PIECIUL E., Vacuum **48** (1997), 293.
[45] MANDELBROT B.B., *The Fractal Geometry of Nature*, San Francisco 1982.
[46] TAKAYASU H., *Fractals in the Physical Science*, Manchester Univ. Press, Manchester, New York 1990.
[47] BOUCHAUD J.P., Proc. Int. Workshop on Lévy Flights and Related Topics in Physics, Nice, France 1995, pp. 27–30.
[48] DOBIERZEWSKA-MOZRZYMAS E., BIEGAŃSKI P., WÓJCIK J. PIECIUL E., J. Phys.: Condens. Matter **11** (1999), 5561.

Received June 20, 2000
in revised form December 12, 2000